Series Expansion Analysis of a Frustrated Four-Spin-Tube

Marcelo Arlego[1] and Wolfram Brenig[2, *]

[1]*Departamento de Física, Universidad Nacional de La Plata, C.C. 67, 1900 La Plata, Argentina*
[2]*Institut für Theoretische Physik, Technische Universität Braunschweig, 38106 Braunschweig, Germany*

We study the magnetism of a frustrated four-leg spin-1/2 ladder with transverse periodic boundary conditions: the frustrated four-spin tube (FFST). Using a combination of series expansion (SE), based on the continuous unitary transformation method and density-matrix renormalization group (DMRG) we analyze the ground-state, the one-, and the two-particle excitations in the regime of strong rung-coupling. We find several marked differences of the FFST with respect to standard two-leg ladders. First we show that frustration destabilizes the spin-gap phase of the FFST which is adiabatically connected to the limit of decoupled rung singlets, leading to a first order quantum phase transition at finite inter-rung coupling. Second, we show that apart from the well-know triplon branch of spin-ladders, the FFST sustains additional elementary excitations, including a singlon, and additional triplons. Finally we find, that in the two-particle sector the FFST exhibits collective (anti)bound states similar to two-leg ladders, however with a different ordering of the spin-quantum numbers. We show that frustration has significant impact on the FFST leading to a flattening of the ground-state energy landscape, a mass-enhancement of the excitations, and to a relative enhancement of the (anti)binding strength. Where possible we use DMRG to benchmark the findings from our SE calculations, showing excellent agreement.

I. INTRODUCTION

Ever since it has been realized that there are 'surprises' on the way from one- to two-dimensional quantum magnets[1], spin ladders have attracted an enormous interest. Two-leg ladders, such as $Sr_{14-x}Ca_xCu_{24}O_{41}$[2], have been under intense scrutiny mainly because of the potential interplay between their spin-gaped ground state and the occurrence of superconductivity[3,4]. N-leg ladders with $N > 2$ are of particular relevance, not only because they allow for a generalized test of Haldane's conjecture[5], but also because new, *tube-like* lattice structures can be realized if periodic transverse boundary conditions apply, such as in $[(CuCl_2tachH)_3Cl]Cl_2$[6] and $CsCrF_4$[7] with $N = 3$, $Cu_2Cl_4 \cdot D_8C_4SO_2$[8,9] with $N = 4$, and $Na_2V_3O_7$[10] with $N = 9$. For $N = 3$, magnetic frustration surfaces as an additional ingredient, already for tubes with only nearest neighbor exchange, leading to a rich variety of phenomena not present in two-leg ladders[11–15]. Experimentally, the four-spin tube $Cu_2Cl_4 \cdot D_8C_4SO_2$ has been suggested to display frustrating antiferromagnetic next-nearest neighbor exchange[8]. Theoretically, *unfrustrated* four-spin tubes have been considered in two seminal papers[16,17], in the weak and the strong rung-coupling limit, and in the context of a broader study of magnetization plateaus in ladders with an arbitrary number of legs. Magnetic frustration, however, has not been considered in these studies. Therefore, in this work, we perform a first analysis of a frustrated four-spin tube (FFST)

$$H = \sum_{lm} j_{lm} \mathbf{S}_l \cdot \mathbf{S}_m \,, \tag{1}$$

with a lattice structure and exchange couplings j_{lm} as shown in Fig.1. Spin-1/2 moments are located on the solid circles and all couplings, j_0, j_1 and j_2 are antiferro-
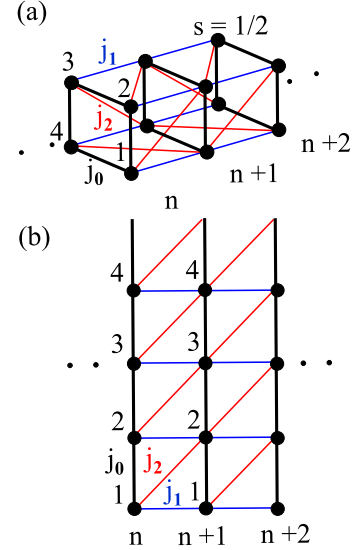

Figure 1: (a) Frustrated four-spin tube. Solid circles represent spin-1/2 moments. Plaquettes (bold black lines) are coupled by nearest (j_1) and next nearest (j_2) antiferromagnetic exchange, blue and red lines. On-plaquette couplings (j_0) are set to unity. (b) Frustrated four-spin tube unrolled, showing the structure of an anisotropic triangular lattice strip.

magnetic (we set $j_0 = 1$ hereafter). This FFST is simpler than the one proposed for $Cu_2Cl_4 \cdot D_8C_4SO_2$, where only part of the surface squares experience diagonal exchange, and the leg-couplings seem to be in-equivalent[8]. Apart its relation to existing materials, the FFST is of interest as a 1D variant of the anisotropic triangular lattice on the torus with four site circumference, i.e. cutting the tube longitudinally one obtains an anisotropic triangular lattice strip. For $j_{1,2} \ll 1$, the FFST resembles a chain

of weakly coupled four-spin plaquettes each of which displays a singly degenerate singlet ground state, separated by a gap of $j_0 = 1$ from the first excited triplet. Therefore perturbation theory in $j_{1,2}$ applies. Motivated by this we investigate the FFST by series expansion (SE) in $j_{1,2}$. Moreover, we corroborate our approach and gauge our SE results by employing density-matrix renormalization group (DMRG) calculations. The structure of the paper is as follows. In section II we clarify the region of applicability of the SE. Section III details our SE method. Results are presented in section IV, including the ground state energy of the FFST in sub-section IV A, the one-particle excitations in sub-section IV B, as well as two-particle states in IV C. Conclusions are presented in section V. For completeness, technicalities of the two-particle SE calculations are included in the appendix VII.

II. COUPLED PLAQUETTE REGIME

Proper application of SE hinges on the adiabatic renormalization of the bare starting state in terms of the coupling constants. In case of intervening second order quantum phase transitions, the SE can be used directly to limit its range of applicability in terms of diverging susceptibilities or vanishing elementary excitation gaps. In case of a discontinuous or first order transitions, SE based on a single bare ground state fails to signal any transition. To put our SE on firm grounds *a-priori*, we therefore search for potential first-order quantum phase-transitions of the FFST at small $j_{1,2}$.

To this end, it is instructive to first consider the classical phase diagram of the FFST. We allow the spin structure to be a spiral, which, due to $SU(2)$ symmetry can be considered to be planar $\mathbf{S} = S(\cos(\mathbf{Q}\cdot\mathbf{r}), \sin(\mathbf{Q}\cdot\mathbf{r}), 0)$ with $\mathbf{r} = l_x\mathbf{R}_x + l_y\mathbf{R}_y$, where $\mathbf{R}_{x,y} = (1,0),(0,1)$, $l_x \in \mathbb{N}$, and $l_y = [1,\ldots 4]$. The transverse pitch vector Q_y has to be discretized according to $(0,1,2,3)\pi/2$. The ground state energy is $e_g^c = \cos(Q_y) + j_1\cos(Q_x) + j_2\cos(Q_x + Q_y)$. From this, four classical phases result, shown in Fig. 2: a (π,π) antiferromagnet for $j_2 \leqslant (1 + 2j_1)/(2(j_1 + 1)), \wedge j_2 \leqslant j_1$ (region A), a $(0,\pi)$ columnar antiferromagnet for $j_2 \geqslant (1 - 2j_1)/(2(j_1 - 1)), \wedge j_2 \geqslant j_1$ and $j_1 < 1$ (region C), a $(\pi,0)$ columnar antiferromagnet for $j_2 \geqslant (2j_1 - 1)/(2(j_1 - 1)), \wedge j_1 > 1$ (region B). In the remaining region D, the energy is minimized by two degenerate incommensurate spirals with pitch $(Q_x, Q_y) = (2\arctan(\alpha), \pi/2)$ and $(2\pi - 2\arctan(\alpha), 3\pi/2)$, and $\alpha = (j_1 + \sqrt{j_1^2 + j_2^2})/j_2$. Due to Q_y's discretization all of the classical transitions are discontinuous.

While the quantum analog of this rather rich phase diagram clearly deserves future analysis, our SE is confined to the region of $j_{1,2} \lesssim 1$. Therefore we focus only this region regarding potential first order quantum phase transitions. First, the classical 'diagonal' transition from the $(0,\pi)$ to the (π,π) state has no quantum analog, since it is connected to the region of $j_{1,2} \ll 1$. There, and instead of the classical (π,π) or $(0,\pi)$ antiferromag-
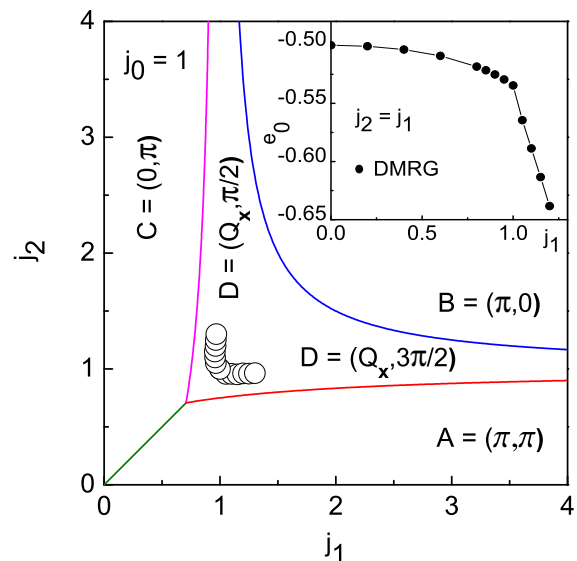

Figure 2: Phase diagram of the FFST. Solid lines: transitions at the *classical* level (all are discontinuous). Wave vectors A, B, C and D label pitch angle of classical phase. Circles: first-order *quantum* critical line from DMRG (see text). Inset: ground state energy versus j_1 from DMRG for the quantum model at $j_2 = j_1$, showing first order transition at $j_1 = j_1^c \approx 1$.

nets, the quantum model shows a phase of weakly coupled plaquette-singlets and the quantum ground state is protected by the singlet-triplet gap of the bare plaquette. To assess the relevance to the quantum case of the classical transitions from the $(0,\pi)$ and (π,π) states into the doubly-degenerate $(Q_x, \pi/2)$, $(Q_x, 3\pi/2)$ phase, we resort to a DMRG analysis of the ground state energy. For this we use the ALPS package[18]. Since we are only concerned with first order transitions, we refrain from any detailed finite size scaling analysis. We find that for $j_{1,2} \lesssim 2$ there is negligible finite size dependence of the ground state energy for FFSTs of lengths $L \approx 30\ldots 40$, i.e. $120\ldots 160$ spins, and that $m = 300\ldots 400$ states kept in the density matrix lead to $4\ldots 5$ digits of precision, which is sufficient for our purpose.

The inset in Fig. 2 shows a typical result for the ground state energy e_0 obtained from DMRG versus j_1 along the diagonal $j_1 = j_2$. Obviously the ground state energy displays a kink at $j_1 = j_1^c \approx 1$, which we identify with a first order transition. The circles in Fig. 2 summarize a scan of locations of this transition which we have performed. The size of the circles is a rough measure of the numerical accuracy for the locations of the transition. These locations are remarkably close to those of the classical model. Below these transitions SE based on decoupled plaquettes is applicable. Beyond $j_{1,2} \sim 1.5$ the critical points are increasingly hard to detect accurately from the DMRG data. We speculate that below the first-order transition lines at $j_1^c(j_2)$ and $j_2^c(j_1)$ the bare plaquette state is adiabatically connected to a Luttinger liquid for $j_2 \to \infty$ and $j_1 \to \infty$, respectively.

State	q_n	E_n	S	S_z	Idx
$|s_0\rangle$	0	-2	0	0	0
$|t_0^{S_z}\rangle$	1	-1	1	-1,0,1	1,2,3
$|s_1\rangle$	2	0	0	0	4
$|t_1^{S_z}\rangle$	2	0	1	-1,0,1	5,6,7
$|t_2^{S_z}\rangle$	2	0	1	-1,0,1	8,9,10
$|q^{S_z}\rangle$	3	1	2	-2,...,2	11,...,15

Table I: Spectrum of the single plaquette. It consists of four equidistant energy levels $E_n = q_n - 2$ labeled by the quantum number $q_n = 0, .., 3$, the total spin S, and its z-component S_z. The last column enumerates the states.

III.   SERIES EXPANSION METHOD

The main focus of this work is on SE in terms of j_1 and j_2, starting from the limit of isolated plaquettes. To this end we decompose the Hamiltonian of the FFST into

$$H = H_0 + V,$$
$$H_0 = \sum_n h_{0,n}, \quad V = V_1 + V_2, \quad (2)$$

where $h_{0,n}$ is the plaquette Hamiltonian at site n

$$h_{0,n} = [\mathbf{S}_1 \cdot \mathbf{S}_2 + \mathbf{S}_2 \cdot \mathbf{S}_3 + \mathbf{S}_3 \cdot \mathbf{S}_4 + \mathbf{S}_4 \cdot \mathbf{S}_1]_n \quad (3)$$

and the perturbation $V = V_1 + V_2$ is given by

$$V_1 = j_1 \sum_n \sum_{i=1}^{4} \mathbf{S}_{i,n} \cdot \mathbf{S}_{i,n+1},$$
$$V_2 = j_2 \sum_n (\mathbf{S}_{1,n} \cdot \mathbf{S}_{2,n+1} + \mathbf{S}_{2,n} \cdot \mathbf{S}_{3,n+1}$$
$$+ \mathbf{S}_{3,n} \cdot \mathbf{S}_{4,n+1} + \mathbf{S}_{4,n} \cdot \mathbf{S}_{1,n+1}). \quad (4)$$

The eigenstates of an isolated plaquette consist of four equidistant energy levels $E_n = q_n - 2$, labeled by the quantum number $q_n = 0, .., 3$, and can be classified according to the total and the z-component of the plaquette spin $\mathbf{S}_n = \sum_{i=1}^{4} \mathbf{S}_{i,n}$. Table I lists that the ground state is a singlet, the first excited state at $q_n = 1$ is a triplet, the $q_n = 2$ sector is composed of a singlet and two triplets, and for $q_n = 3$ one quintet remains.

In turn, H_0 displays an equidistant spectrum, labeled by $Q = \sum_n q_n$. At $V = 0$, the $Q = 0$ sector refers to the unperturbed singlet ground state $|0\rangle = \otimes_n |s_{0,n}\rangle$ composed of $q_n = 0$ singlets on all plaquettes. The $Q = 1$ sector comprises single $|t_{0,m}^{S_z}\rangle$ triplets inserted into $|0\rangle$ at site m. The $Q \geq 2$ sectors are of multi-particle nature. The perturbation V can be rewritten as $V = \sum_{i=1}^{2} j_i \sum_{n=-N}^{N} T_n^i$, where T_n represent raising ($n > 0$) or lowering ($n < 0$) operators within the spectrum of H_0. For the FFST we find $N = 4$.

It has been shown quite generally[19], that models with the preceding type of spectrum allow for SE through a continuous unitary transformation (CUT) using the flow equation method of Wegner[20]. The basic idea is to transform H onto an effective Hamiltonian H_{eff} which is
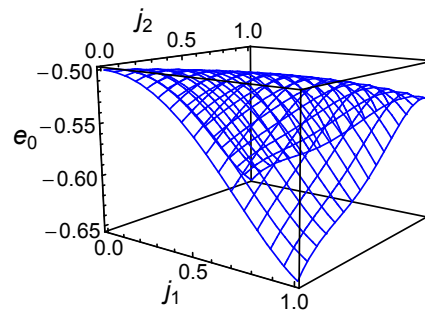

Figure 3: Ground state energy per site e_0 versus j_1 and j_2, showing a monotonously decreasing behavior in the parameter range shown. Along the line of maximum frustration $j_1 = j_2$, the energy gain is smallest.

block-diagonal in the quantum number Q. This transformation can be achieved exactly order-by-order in $j_{1,2}$ leading to

$$H_{\text{eff}} = H_0 + \sum_{n,0 \leq m \leq n} C_{n,m} j_1^{n-m} j_2^m, \quad (5)$$

where the $C_{n,m}$ are weighted products of the T_n^i operators which conserve the Q-number and have their weights determined by recursive differential equations, see[19] for details. Due to Q-number conservation several observables can be accessed directly from H_{eff} in terms of a SE in $j_{1,2}$. For systems with coupled spin-plaquette CUT SE has been used for one[21], two[22–25] and three[26] dimensions.

IV.   RESULTS

In this Section we present our findings from SE up to $Q = 2$, sectioning the discussion according to A. the ground-state energy, B. the one-, and C. the two-particle excitations. To assess the quality of the SE we complement our analysis by DMRG calculations for selected cases.

A.   Ground State Energy

First we consider the ground state energy E_0. Q-conservation leads to

$$E_0 = \langle 0|H_{\text{eff}}|0\rangle, \quad (6)$$

where $|0\rangle$ is the unperturbed ground state.

Evaluating this matrix element on chains with periodic boundary conditions (PBC) of a length L, sufficient not to allow for wrap-around of graphs with length N, i.e. $L = N + 1$, one can obtain analytic SEs which are valid to $O(N)$ with respect to eqn. (5) in the thermodynamic limit. Evaluating the ground state energy per spin $e_0 =$

$E_0/(4L)$ up to $O(7)$ we get

$$
\begin{aligned}
e_0 = &-\frac{1}{2} - \frac{17}{96}\left(j_1^2 + j_2^2\right) + \frac{1}{3}j_1 j_2 + \frac{1}{16}\left(j_1^2 j_2 + j_1 j_2^2\right) \\
&- \frac{25}{384}\left(j_1^3 + j_2^3\right) + \frac{1919}{96768}\left(j_1^4 + j_2^4\right) + \frac{15457}{48384}j_1^2 j_2^2 \\
&- \frac{313}{1728}\left(j_1^3 j_2 + j_1 j_2^3\right) + \frac{1510499}{27095040}\left(j_1^5 + j_2^5\right) \\
&- \frac{39353}{188160}\left(j_1 j_2^4 + j_1^4 j_2\right) + \frac{4129273}{27095040}\left(j_1^3 j_2^2 + j_1^2 j_2^3\right) \\
&+ \frac{522374480359}{14748372172800}\left(j_1^6 + j_2^6\right) + \frac{9888732599}{17069875200}j_1^3 j_2^3 \\
&- \frac{1494532466633}{4916124057600}\left(j_1^4 j_2^2 + j_1^2 j_2^4\right) \\
&- \frac{92947333}{4267468800}\left(j_1^5 j_2 + j_1 j_2^5\right) \\
&+ \frac{3149204376698497}{12388632625152000}\left(j_1^6 j_2 + j_1 j_2^6\right) \\
&+ \frac{1186859862395537}{2753029472256000}\left(j_1^4 j_2^3 + j_1^3 j_2^4\right) \\
&- \frac{274272578154571}{412954420838400}\left(j_1^5 j_2^2 + j_1^2 j_2^5\right) \\
&- \frac{535161937582507}{24777265250304000}\left(j_1^7 + j_2^7\right)
\end{aligned} \tag{7}
$$

Here, the first term corresponds to the bare energy per spin listed in table I. Since the FFST can be mapped onto an identical FFST with $j_1 \leftrightarrow j_2$ by a $\pi/2$-twist of the plaquettes around the tube, one expects that $e_0(j_1, j_2) = e_0(j_2, j_1)$, which is obviously fulfilled. Figure 3 shows $e_0(0 \leq j_1 \leq 1, 0 \leq j_2 \leq 1)$ to be monotonously decreasing with $j_{1,2}$. Along the line $j_1 = j_2$, the energy gain is smallest. Speaking differently, along its maximally frustrated direction in parameter space the energy landscape is flattest.

In Fig. 4 we asses the accuracy of eqn. (7) in several ways. First, in panel (a) we compare e_0 with DMRG calculations along $j_2 = 0$ where we expect no first-order transition. The DMRG results have been obtained for $L = 30$ and $m = 300$. Obviously the agreement between SE and DMRG is very good for $j_1 \lesssim 0.75$. In panel (b) we display a similar comparison along $j_1 = j_2$. Here the SE agrees very well with DMRG to even larger values of $j_{1,2}$, however only up to the first-order transition discussed in section II. Third, in panel (a) we also include three DlogPadé approximants to eqn. (7), which, similar to the DMRG, start to depart from the SE for $j_1 \gtrsim 0.75$ and may be used to increase the interval of confidence of the SE only slightly by $\sim 10\%$ as evident from the DMRG results. For reference panel (a) also depicts the ground state energy per site of the 1D HAFM with exchange constant j_1 which is $(-\ln(2) + 1/4)j_1$. Evidently, in the parameter range we consider, the FFST is far away from the decoupled chain limit.
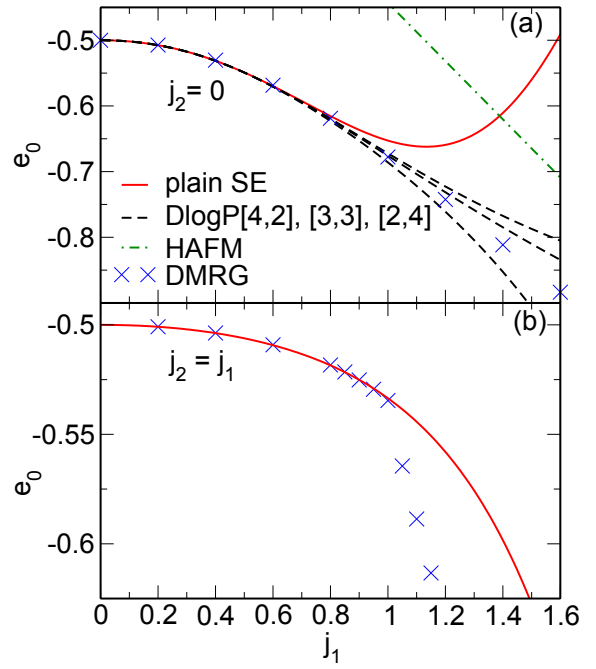

Figure 4: (a) Comparison between e_0 from plain SE (red solid lines) with DMRG for $L = 30$ and $m = 300$ (blue crosses), along $j_2 = 0$. Black dashed lines refer to three DlogPadé approximants to eqn. (7). For reference the ground state energy of the 1D HAFM is also depicted (green dash-dotted). (b) Comparison of plain SE (red solid lines) with DMRG (blue crosses) along $j_1 = j_2$. Up to the first-order transition discussed in section II, the agreement is excellent.

B. One-particle Excitations

Now we turn to the dispersion of one-particle eigenstates. By the latter we mean excited eigenstates of the effective Hamiltonian which, apart from having fixed Q, lattice momentum k, and total spin quantum numbers S, m, are linear combinations of *single* entries of table I only. $Q = 1$ eigenstates are single particle states by construction. For $Q \geqslant 1$, Q-conservation does not protect single states in table I from decay into *two* states by virtue of H_{eff}. Eg. a $|s_{1l}\rangle$ singlet with $Q = 2$ at site l could decay into two $|t_{0i(j)}^{S_z}\rangle$ triplets with total spin $S = 0$ and $Q = 1 + 1$ at sites $i(j)$ (see also appendix VII). For the FFST however, and for $Q = 2$, $S = 0, 1$ and up to $O(7)$, we find that all matrix elements of H_{eff} inducing such decay *vanish* identically. This feature can be traced back to the C_4 symmetry of the tube. In fact, we obtain that changing e.g. the exchange couplings j_1 into $j_1' \neq j_1$ on one of the legs, renders the one-particle $Q = 2$ states unstable against decay. In summary, for each momentum k the $Q = 2$ spectrum contains three genuine one-particle levels with $S = 0, 1$, all of which are degenerate in m. For the remaining *two*-particle states with $Q = 2$ we refer to the next section.

For the rest of this section we label the one-particle states by $|i\rangle^{Q, S_n}$, where i refers to the plaquette's site

and S_n is the total spin, where the index n is only due to the fact that for $Q = 2$ there are two $S = 1$ states, say, $n = a, b$. Spin-z quantum numbers m are discarded because of $SU(2)$ invariance. Due to Q-conservation and $SU(2)$ invariance the effect of H_{eff} on $|i\rangle^{Q,S_n}$ is limited to

$$H_{\text{eff}}|j\rangle^{Q,S_n} = \sum_{i, S_n = S_m} t_i^{Q,S_n,S_m} |j+i\rangle^{Q,S_m}, \qquad (8)$$

which implies a shift in real space, and potentially a mixing of states of equal S with identical Q. The hopping amplitudes t_i^{Q,S_n,S_m} do not depend on j due to translation invariance. Therefore, by Fourier transformation $|k\rangle^{Q,S_n} = 1/\sqrt{L} \sum_j \exp(-i\,k\,j)|j\rangle^{Q,S_n}$ we get the dispersion from

$$E_{Q,S_n,S_m}^{\text{1pt}}(k) = {}^{Q,S_n}\langle k|H_{\text{eff}}|k\rangle^{Q,S_m} - E_0\,\delta_{S_n,S_m}$$
$$= \tilde{t}_0^{Q,S_n,S_m} + 2\sum_i t_i^{Q,S_n,S_m} g(ik), \qquad (9)$$

where, obviously $t_i^{Q,S_n,S_m} = t_{-i}^{Q,S_n,S_m}$ for $S_n = S_m$. However for $S_n \neq S_m$, i.e. for the two $Q = 2$, $S = 1$ states, we find $t_i^{Q,S_n,S_m} = -t_{-i}^{Q,S_n,S_m}$. In turn, $g(x)$ is $\cos[i\sin](x)$ for S_n-[off]diagonal transitions.

To obtain hopping amplitudes valid to $O(N)$, in the thermodynamic limit, the t_i^{Q,S_n,S_m} and the ground state energy $E_0 = \langle 0|H_{\text{eff}}|0\rangle$ in eqn.(9) have to be evaluated on clusters with open boundary conditions (OBC), large enough to incorporate N-th order graphs for hopping processes of distance i[19]. Depending on i, these clusters are of either of length N or $N+1$. We have calculated *analytic* expressions[27] for $E_{Q,S_n,S_m}^{\text{1pt}}(k)$ to $O(7)$ in $j_{1,2}$. For $(Q,S) \neq (2,1)$ eqn. (9) is already diagonal in S_n, S_m with eigenvalues $E_{Q,S_n}^{\text{1pt}}(k) \equiv E_{Q,S_n,S_n}^{\text{1pt}}(k)$. Only for $(Q,S) = (2,1)$ eqn. (9) displays a 2×2-matrix structure, referring to $n = a, b$, with eigenvalues $E_{Q,1a}^{\text{1pt}}(k)$ and $E_{Q,1b}^{\text{1pt}}(k)$.

In Fig. 5 we show the one-particle dispersions for selected values of $j_{1,2}$. This figure displays only bare SE results and no Padé extrapolations. Several comments are in order. First, the figure does not only display $E_{Q,S_n}^{\text{1pt}}(k)$ for all S and $Q \leq 2$, but for curiosity also the quintet with $Q = 3$, assuming that the latter does not decay into multi-particle states - which we have not checked.

As for the ground state energy, since exchanging $j_1 \leftrightarrow j_2$ maps the FFST onto an equivalent one by a $\pi/2$-twist there are related symmetries of the one-particle dispersions. These respect the additional fact, that the single-particle states on the bare plaquette are the eigenstates of a four-site spin-1/2 chain with PBC, which carry one out of four momenta $k_{n\perp} = n\pi/2$ with $n = 0, 1, 2, 3$ transverse to the FFST. In turn, exchanging $j_1 \leftrightarrow j_2$ maps the one-particle dispersions onto identical ones up to a shift of the Brillouin zone by one out of $k_{n\perp}$, and may also exchange the dispersion branches for the degenerate bare $Q, S = 2, 1$ states. We have checked this to be fulfilled by all $E_{Q,S_n}^{\text{1pt}}(k)$. Eg., for $(Q, S) =$
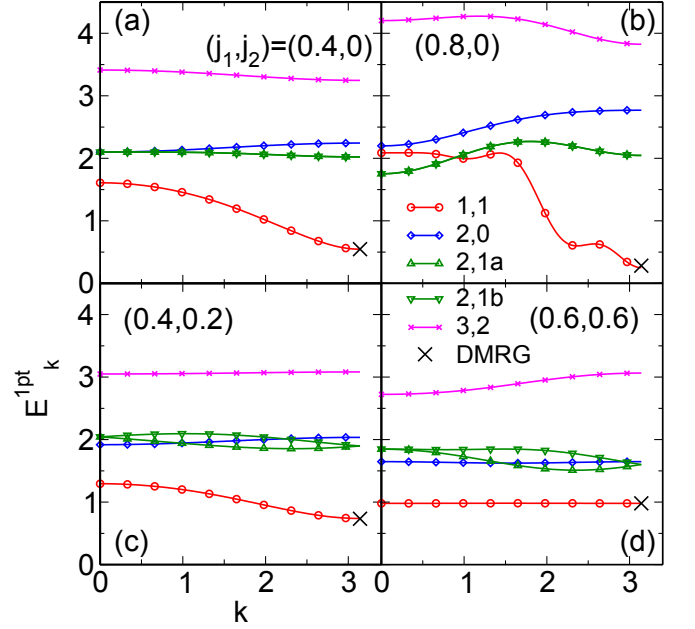

Figure 5: Genuine one-particle dispersions on the FFST for $Q \leq 2$ at various values of (j_1, j_2). These comprise three triplets (red circle, green triangle up, green triangle down) and one singlet (blue diamond). The Q=3-quintet (magenta x) has not been tested against multi-particle decay and is only shown for reference. DMRG results at zone-boundaries are shown with large crosses.

$(1, 1)$ we have $E_{Q,S_n}^{\text{1pt}}(k, j_1, j_2) = E_{Q,S_n}^{\text{1pt}}(k + \pi, j_2, j_1)$ and for $(Q, S) = (2, 1a[b])$ we have $E_{Q,1a[b]}^{\text{1pt}}(k, j_1, j_2) = E_{Q,1b[a]}^{\text{1pt}}(k+[-]\pi/2, j_2, j_1)$. Additionally $E_{Q,1a[b]}^{\text{1pt}}(k, j_1, j_2)$ are degenerate at $j_2 = 0$.

Considering the elementary triplet dispersion $E_{1,1}^{\text{1pt}}(k)$ at $j_2 = 0$, we observe a zone-boundary gap in Fig. 5 (a) which decreases as j_1 increases, see panel (b). For four-leg ladders without frustration, i.e. $j_2 = 0$, the analytic expression for the gap we get is

$$E_{1,1}^{\text{1pt}}(\pi, j_1, 0) = 1 - \frac{4}{3}j_1 + \frac{41}{108}j_1^2 + \frac{349}{1296}j_1^3$$
$$+ \frac{4596401}{39191040}j_1^4 - \frac{169497997}{4702924800}j_1^5$$
$$- \frac{689874137639377}{2986545364992000}j_1^6$$
$$- \frac{8430165345498432721}{45156565918679040000}j_1^7, \qquad (10)$$

which, in passing, improves earlier SE to $O(4)$ on *unfrustrated* four-leg ladder[16] by three orders. The dispersion $E_{1,1}^{\text{1pt}}(k)$ shows rather strong oscillations in panel (b). These are not related to convergence issues of the SE, but are robust features of hopping to more than only nearest-neighbors.

Increasing j_2 from zero, at fixed j_1, as from Fig. 5 (a) to (c) the bandwidth of $E_{1,1}^{\text{1pt}}(k)$ is reduced. On the line of maximum frustration, i.e. at $j_1 = j_2$ in panel (d), it is

S	$\|ij\rangle^{Sm}$, $\|i\rangle^{Sm}$
2	$\sum_n C_{1n,1m-n}^{2m} \|t_{0i}^n t_{0j}^{m-n}\rangle$
1	$\sum_n C_{1n,1m-n}^{1m} \|t_{0i}^n t_{0j}^{m-n}\rangle$, $\|t_{1i}^m\rangle$, $\|t_{2i}^m\rangle$
0	$\sum_n C_{1n,1m-n}^{00} \|t_{0i}^n t_{0j}^{m-n}\rangle$, $\|s_{1i}\rangle$

Table II: $Q = 2$ states from the bare plaquette. $C_{1n,1m-n}^{Sm} = \langle 1n, 1m-n|Sm\rangle$ are Clebsch-Gordan coefficients.

only very small, albeit *not* exactly zero, namely $O(j_1^4)$. A similar tendency can be observed in all other (Q, S) sectors, yet less pronounced. We note that in the vicinity of the first-order transition, and on the line $j_1 = j_2$, the one-particle gap from SE is practically identical to the one shown in Fig. 5 (d), i.e. no gap-closure occurs at the first-order transition depicted in Figs. 2 and 4 (b).

To assess the quality of the SE, we have also calculated the elementary $(Q, S) = (1, 1)$ gap by DMRG. The results are shown by the large crosses at the zone-boundaries in Fig. 5. As is obvious, the agreement is very good in all four panels. This is particularly noteworthy for panel (b), corroborating the preceding statement, that the oscillations in $E_{1,1}^{1pt}(k)$ for larger values of j_2 are robust features of the SE and no convergence issue.

C.   Q=2 Two Particle States

In this section we focus on two-particle states generated from two one-particle triplets out of the $(Q, S) = (1, 1)$ sector. Apart from generating a continuum of states at fixed total momentum with respect to the relative momentum, interactions may lead to additional collective (*anti*)*bound states* which split off from the continuum. The existence of such collective states is know for simpler 1D quantum magnets, such as chains and two-leg ladders[28–34]. Here we show that similar states exist also on the FFST. To this end we evaluate the two-particle spectrum following ideas developed for dimer-SE of two-leg ladders[33]. For the sake of completeness technical details of this procedure are revisited in appendix VII.

On the FFST, the $Q = 2$ sector allows for one-particle *and* two-particle states. This is different from dimer systems where only two-particle states occur for $Q = 2$[33]. The real-space representations of all $Q = 2$ states with proper spin quantum numbers S, m are listed in table II. Here the genuine two-particle states are labeled by $|i, j\rangle^{Sm}$, where i, j refers to sites on the 1D lattice and S, m to total spin, and spin-z quantum numbers. As discussed in the preceding section the one- and two-particle excitations at $Q = 2$ do not mix. Therefore we focus on the genuine two-particle excitations hereafter.

Because of translational invariance the two-particle states can be classified according to a center-of-mass momentum q and a relative distance d

$$|q, d\rangle^{Sm} = \frac{1}{\sqrt{L}} \sum_r e^{iq(r+d/2)} |r, r + d\rangle^{Sm} \qquad (11)$$
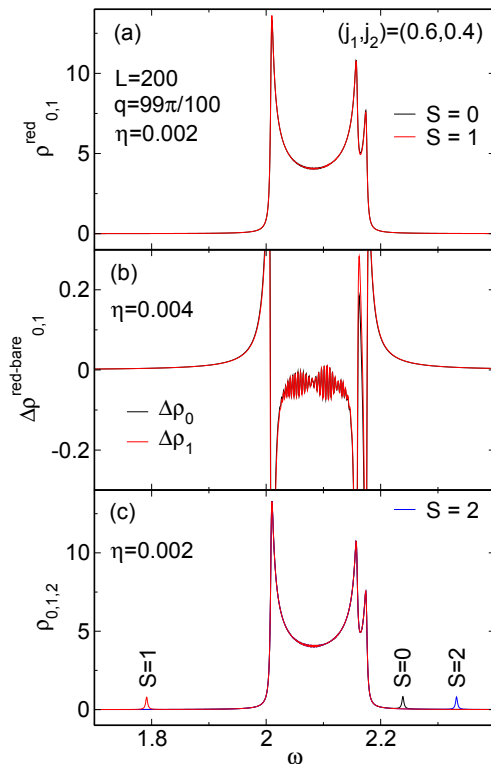

Figure 6: Two-particle density of states close to the zone boundary at $q = 99\pi/100$ on an $L = 200$ site FFST for $(j_1, j_2) = (0.6, 0.4)$. Delta functions at each two-particle energy broadened by η. (a) *reducible* spectrum for S=0 and S=1. (b) difference between bare and *reducible* spectrum for S=0 and S=1. (c) complete spectra for S=0,1,2.

These states have an exchange parity $P = (-1)^S$ for $d \to -d$, i.e. $|q, -d\rangle^{Sm} = P|q, d\rangle^{Sm}$. The effective Hamiltonian, eqn. (5), will mix states at different d. The two-particle spectrum is obtained from the sum of the one- and two-particle irreducible Hamiltonians (see[31,33] and appendix VII), labeled by H_1 and H_2, with *analytic* matrix elements calculated by SE from the states of eqn. (11). We have evaluated these matrix elements to $O(6)$. For each q, this leads to an eigenvalue problem with a rank set by the number of lattice sites (or relative momenta) L. This can be diagonalized numerically on finite, but large lattices. See appendix VII for definitions and formal details.

In Fig. 6 we show the two-particle spectrum $\rho_S(q, \omega) = \sum_p \delta(\omega - E_{S,m}^{2pt}(q, p))$ at fixed total momentum q and spin S, m, summed over the relative momentum p, where $E_{S,m}^{2pt}(q, p)$ are the two-particle eigenenergies. We choose $(j_1, j_2) = (0.6, 0.4)$ and $q \simeq \pi$ as an example. To analyze the effects of the interaction we consider $E_{S,m}^{2pt}(q, p)$ at various levels of approximation. First, we set the irreducible two-particle interactions H_2 to zero - i.e. no 'actual' interactions occur. The corresponding spectrum is shown in Fig. 6 (a) for $S = 0$ and $S = 1$. These spectra are indistinguishable on the scale of this plot. The
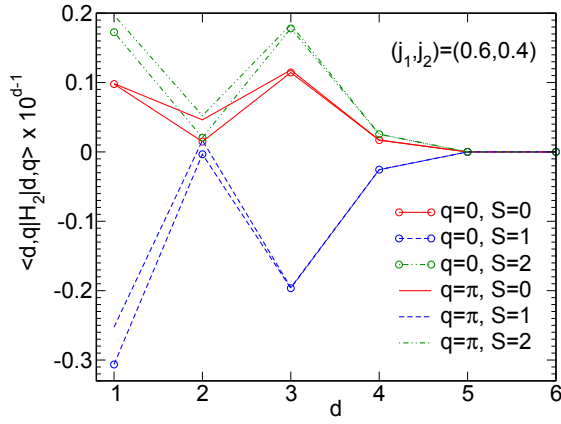
Figure 7: Diagonal element of the irreducible interaction $\langle q, d|H_2|q, d\rangle$ versus relative distance of two particles for $S = 0, 1$, and 2, and for $q = 0$ and π, multiplied by 10^{d-1}. (The matrix elements of H_2 at $O(6)$ are zero for $d = 5, 6$.)

van-Hove singularities are related to the extrema of the one-particle dispersion in the $(Q, S) = (1, 1)$ sector as in Fig. 5. Even though the irreducible one-particle interaction H_1 will act only on one of the two particles, this does *not* imply, that the spectra in Fig. 6 (a) are identical to the convoluted *bare* spectra of two *single* $|t_0^{S_z}\rangle$-particles at fixed total momentum q and finite L. This is due to the hard-core constraint which forbids double occupation of plaquettes by $|t_0^{S_z}\rangle$-particles. This constraint is encoded in the matrix elements of H_1 when acting on the two particle sector. Since there are L double occupancies within L^2 two-particle states, their removal amounts to a $1/L$ effect on the integrated spectral weight at fixed total momentum q. At fixed total and relative momentum, this effect will be *quantitatively* identical for two-particle states of identical exchange parity $(-)^S$. For this reason Figs. 6 (a) and (b) contain only $S = 0$ and 1 sates. Figure 6 (b) depicts the difference between the *bare* spectra and that obtained from H_1 for $S = 0$ and $S = 1$ for $L = 200$. Clearly the integrated spectral weight for both values of S is finite but of $O(1/L)$ at most. Differences are visible between the $S = 0$ and $S = 1$ spectrum - albeit very small. Figure 6 (a) shows that *no* (anti-)bound state arises in the two-particle sector solely due to the hard-core repulsion.

Next we consider the complete $Q = 2$ spectrum in Fig. 6 (c) for $S = 1, 2$ and 3, including the irreducible two-particle interaction H_2. The latter is *spin-dependent* and *longer-ranged*. This figure clearly demonstrates a main point of this section, i.e. the occurrence of three split-off (*anti*)-*bound* states (above) below the continuum depending on their spin. Apart from that, and similar to the hard-core constraint H_2 leads to an $O(1/L)$ redistribution within the two-particle continuum. The total momentum q in Fig. 6 has been chosen, such as to evidence the (anti)-bound states clearly. Depending on q they can approach and also merge with the continuum.
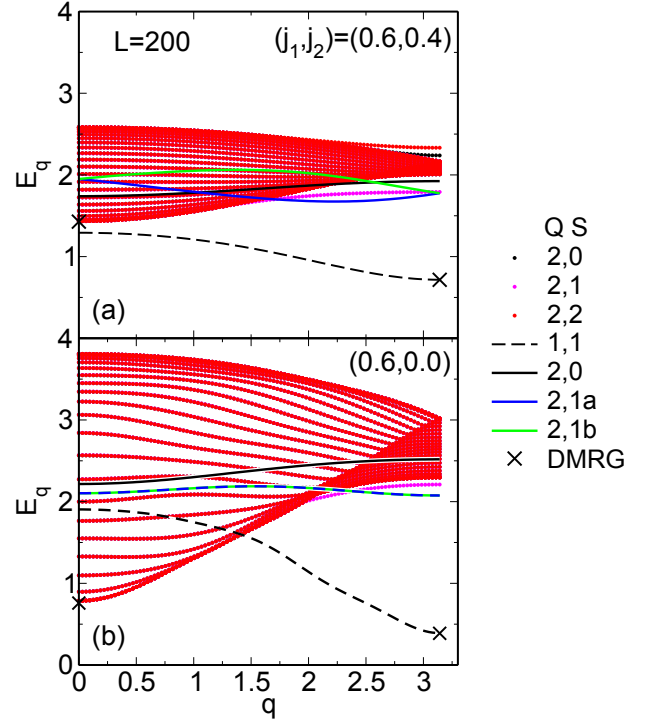
A qualitative understanding of binding versus anti-

Figure 8: Momentum resolved spectrum of all states on the FFST with $Q \leq 2$ for $(j_1, j_2) = (0.6, 0.4)$ and $(0.6, 0)$. Apart from four genuine one-particle states, i.e. three triplets (black dashed, blue solid, green solid), and one singlet (black solid), there are three two-particle continua with S=0,1,2, and three collective two-particle states: a bound triplet (magenta dots), an anti-bound singlet (black dots) and an anti-bound quintet (red dots). Only $\sim 10\%$ of the scattering states between the lower and upper bounds of the continua are depicted to avoid graphic cluttering. DMRG results for one and two-particle states at zone-boundaries(centers) are depicted with large crosses.

binding of the collective two-particle states can be obtained from considering the diagonal matrix elements $^{Sm}\langle q, d|\, H_2|q, d\rangle^{S'm'}$ of two particles versus their relative distance d at fixed total momentum q. This matrix element is $\propto \delta_{S'S}\delta_{m'm}$ and independent of m. It is shown in Fig. 7 for $j_{1,2}$ identical to that of Fig. 6. First, this figure demonstrates that the irreducible two-body interactions are very rapidly decaying as a function of the relative distance of the particles (note the scaling of the matrix elements by 10^{d-1} on the y-axis). Second, and for both total momenta depicted, the interactions for $S = 1$ are attractive, while those for $S = 0, 2$ are repulsive. This is consistent with binding versus anti-binding of the collective states in Fig. 6. Yet, one should keep in mind the matrix elements $^{S'm'}\langle q, d' \neq d|\, H_2|q, d\rangle^{Sm}$ which are off-diagonal in d', d. We have not tested if these invalidate the simplified argument given here. Finally, we emphasize, that the ordering of anti-bound versus bound states on the FFST is different from that on plain two-leg ladders. In the latter case two-particle singlets also form

bound states with a binding energy larger than that of the two-particle triplets.

In Fig. 8 we show the dispersion of all one and two-particle states from the $Q = 1$ and $Q = 2$ sector as a function of total momentum for two sets of $j_{1,2}$, obtained by SE, together with DMRG results for one and two-particle states at the zone-boundary(center). This figure is another main result of our paper and summarizes several aspects. First, the spectrum is very rich and consists of various discrete states and three superimposed two-particle continua. This should be contrasted against plain two-leg ladders, which show a less involved low-energy spectrum[29,33]. Some of the discrete states are genuine one-particle states and some are collective two-particle states. For the parameters depicted, the collective two-particle states are clearly visible only close to the zone boundary. The potential existence of critical parameters $j_{1,2}^c$ or wave-vectors q^c for which the collective states merge with the continua is unclear at present. The $Q = 2$ one-particle states are contained almost completely within the spectral range of the continua and split off from the latter only in a range of q similar to the collective states. This situation is also very different from two-leg spin-ladders in which the states which split off from the continuum close to the zone boundary are collective (anti-)bound states only. From an experimental point of view this may pose a challenge on discriminating between such genuine one-particle and collective two-particle states. Finally, the effects of frustration are clearly visible in going from Fig. 8 a) to b): the complete spectrum shows a tendency to localize. However, in contrast to the one-particle dispersions the two-particle interactions are *not* reduced approaching the line of maximum frustration, $j_1 = j_2$. In turn the relative splitting of the collective states from the continuum is enhanced by frustration.

To conclude this section we provide some measure of convergence of the SE for the two-particle continuum in Fig. 9. This figure shows the relative change in energy of all two-particle states at a fixed total momentum versus their energy when switching from an $O(6)$ to an $O(7)$ evaluation of the matrix elements of $H_{1,2}$. For this we confine ourselves to $S = 0$. As is obvious, the changes are completely negligible and fully justify the use of $O(6)$ SE for the two-particle states. We note in passing, that $O(7)$ SE will not only lead to longer-range irreducible one-particle hoppings, but also increase the range of the irreducible two-particle interactions in Fig. 7, retaining however the rapid decay with distance depicted there.

V. CONCLUSIONS

To summarize, we have studied a frustrated four-spin tube, equivalent to an anisotropic triangular lattice on the torus with a four site, plaquette-type of circumference. The focus of our work has been on the regime of strong coupling on the plaquettes, which is adiabatically
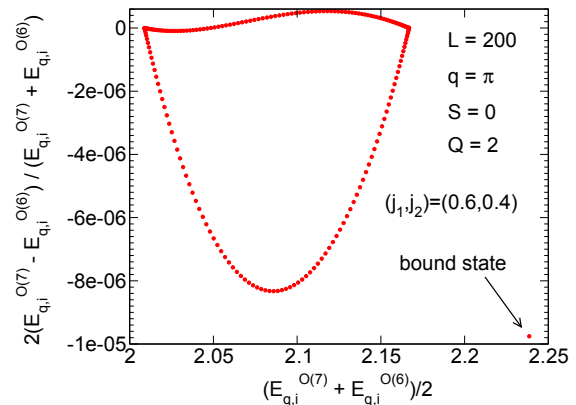

Figure 9: Relative error in all two-particle energies for an FFST of 200 plaquettes at fixed total momentum q for switching from $O(6)$ to $O(7)$ SE. (The apparent 'two-curve' structure is due to an oscillation of the error.)

connected to a pure singlet product state for vanishing exchange $j_{1,2}$ along the tube direction. Our DMRG calculations show the strong coupling regime to be bounded by a line of first order quantum-phase transitions at finite $j_{1,2}$, with a range of stability which depends sensitively on the frustration and displays its smallest extent along the line of maximum frustration, i.e. $j_1 = j_2$. The nature of the phases beyond the transition remains to be explored. For $j_{1,2} \lesssim 1$ we have performed SE calculations for the ground-state energy, the one-, and the two-particle excitations. The gain in ground-state energy, induced by quantum fluctuations, turns out to be suppressed by frustration, leading to an almost flat energy functional along the line $j_1 = j_2$. The energy determined by SE agrees excellently with DMRG. The one-particle sector displays a rich set of elementary excitations including three non-degenerate triplets, one singlet, and possibly a quintet. Part of these excitations will decay into multi-particle states upon reducing the symmetry of the tube's Hamiltonian. Frustration directly influences the kinetic energy of the elementary excitations, decreasing the bandwidth to almost zero along the line of maximum frustration. At weak frustration, effective hopping to more distant neighbors can be strongly enhanced by increasing the exchange along the tube, leading to significant oscillations in the one-particle dispersions. Within the range of $j_{1,2}$ investigated, the one-particle gaps determined from SE shows convincing agreement with DMRG. In the two-particle sector, several scattering-state continua can be observed, which stem from two one-particle excitations. The gaps of these continua match perfectly between SE and DMRG. In addition to that, two-particle interactions lead to three total spin-(0,2)1 (anti)bound collective states, which split off from the continua close to the zone boundary. While for strong frustration the width of the scattering continua decreases, in accordance with the one-particle kinetic energy, the two-particle interactions are less sensitive to frustration. This leads to a

larger splitting of the collective states from the continua at larger frustration. Finally, as compared to a potential material realization of the frustrated four spin tube in $Cu_2Cl_4 \cdot D_8C_4SO_2$, several extensions have to be considered in the future. These comprise e.g. reducing the C_4-symmetry and considering the weak rung-coupling limit.

VII.   EFFECTIVE HAMILTONIAN MATRIX IN THE $Q = 2$ SECTOR

In this appendix we list some of the details necessary to evaluate the two-particle matrix elements by SE. First, we refer to the parity of the states in eqn. (11). Because of this we may confine ourselves to $d > 0$ ($d = 0$, i.e. $|r, r\rangle^{Sm}$ is forbidden). The matrix elements of the one(two)-particle irreducible Hamiltonian $H_{1(2)}$ are obtained by subtracting the one(two)-particle reducible contributions from the matrix elements of H_{eff}[31,33]

$$t_{0,n} = t_{n,0} = \langle n|H_1|0\rangle = \langle n|H_{eff} - H_0|0\rangle \quad (12)$$
$$a_{0,n}^{cl} - \delta_{0,n}E_0^{cl}$$

$$
\begin{aligned}
t_{d|n,d'} &= \langle n, n+d'|H_2|0, d\rangle \quad (13)\\
&= \langle n, n+d'|H_{eff} - H_1 - H_0|0, d\rangle\\
&= a_{d|n,d'}^{cl} - \delta_{0,n}\delta_{d,d'}E_0^{cl} - \delta_{d,n+d'}t_{0,n}^{cl} -\\
&\quad \delta_{0,n}t_{d,n+d'}^{cl} - P\delta_{d,n}t_{0,n+d'}^{cl} - P\delta_{0,n+d'}t_{d,n}^{cl}
\end{aligned}
$$

Here $a_{0,n}^{cl} = \langle n|H_{eff}|0\rangle$, $a_{d|n,d'}^{cl} = \langle n, n+d'|H_{eff}|0, d\rangle$ and cl refers to the cluster on which these matrix elements are evaluated. For $t_{0,n}$ and $t_{d|n,d'}$ to be size consistent, the cluster has to be the largest linked cluster for a given one- and two-particle state in real space at a given order N of the SE. The $t_{0,n}^{cl}$ in eqn. (13) refers to $t_{0,n}$ evaluated on the *same* linked cluster 'cl' as the $a_{d|n,d'}^{cl}$ corresponding to a given $t_{d|n,d'}$ and $E_0^{cl} = \langle 0|H_0|0\rangle$ is the ground state energy of that cluster. The two-particle spectrum results from the eigensystem of

$$^S\langle q, d'|H_{eff} - H_0|q, d\rangle^S = {}^S\langle q, d'|H_2 + H_1|q, d\rangle^S \quad (14)$$

which, due to translational and spin-rotational invariance is diagonal in $q, S,$ and m and is independent of m. For each (q, S, m) the two matrices on the left of eqn. (14) are hermitian with, matrix-indices (d', d). Thus, for the remainder we may consider only $d' \leqslant d$. We begin with $h_{2d'd} = {}^S\langle q, d'|H_2|q, d\rangle^S$. Because a linked cluster can have at most $N + 1$ sites, $h_{2d'd} = 0$ for $d', d > N$. I.e. $h_{2d'd}$ is an $N \times N$ matrix. The action of H_2 is

$$
\begin{aligned}
H_2|q, d\rangle^S &= \frac{1}{\sqrt{L}} \sum_r e^{iq(r+d/2)} \times\\
&\quad \sum_{\max(n+d', d-n) \leqslant N} t_{d|n,d'}|r+n, r+n+d'\rangle^S\\
&= \sum_{\max(n+d', d-n) \leqslant N} t_{d|n,d'} e^{iq((d-d')/2-n)}|q, d'\rangle^S \quad (15)
\end{aligned}
$$

here n must be restricted to $\max(n + d', d - n) \leqslant N$, because of the sites $(0, d, n, n + d')$ to reside within a linked cluster at order N. I.e. n is confined to the interval $d - N \leqslant n \leqslant N - d'$, which has its midpoint at $n_m = (d - d')/2$

$$
\begin{aligned}
H_2|q, d\rangle^S = \{ &\sum_{\substack{\max(n+d', d-n) \leqslant N\\ n=(d-d')/2 \in \mathbb{Z}}} t_{d|(d-d')/2, d'} + \quad (16)\\
&\sum_{\substack{\max(n+d', d-n) \leqslant N\\ n>(d-d')/2 \in \mathbb{Z}}} 2t_{d|n,d'} \cos[q(\frac{d-d'}{2} - n)]\}|q, d'\rangle^S
\end{aligned}
$$

where $t_{d|n,d'} = t_{d|d-d'-n,d'}$ has been used, which refers to reflection symmetry of the two-particle matrix element about the midpoint, and the addends with matrix elements $t_{d|(d-d')/2, d'}$ occurs only if $n_m = (d - d')/2 \in \mathbb{Z}$.

Next, we apply H_1 to a two-particle state. This will only shift one of the particles, i.e.

$$
\begin{aligned}
H_1|q, d\rangle^S &= \sum_{\substack{-N \leqslant n \leqslant N\\ n \neq d}} t_{0,n}^{cl}(e^{-iqn/2} + e^{iqn/2})\\
&\quad \times \frac{1}{\sqrt{L}} \sum_r e^{iq(r+(d-n)/2)}|r, r+d-n\rangle^S\\
&= \sum_{\substack{-N \leqslant n \leqslant N\\ n \neq d}} 2t_{0,n}^{cl} \cos(\frac{nq}{2}) \mathsf{sgn}(d-n)^S|q, |d-n|\rangle^S
\end{aligned}
$$
(17)

For each q, H_1 connects states d and $|d - n|$, $\forall -N \leqslant n \leqslant N$. This is equivalent to a band-matrix of width $2N + 1$. For $d \geqslant N$, the non-zero content of the columns of this matrix is independent of d, for $1 \leqslant d < N$ this is not so. The latter relates to the exclusion of on-site double-occupation.

For reference we explicitly display one specific low-order matrix element $^S\langle q, d'|H_1 + H_2|q, d\rangle^S$ from eqns. (14, 16, 17), namely $d' = d = 1$, $N = 4$ and $S = 0$. Figure 10 relates to the two-particle irreducible matrix
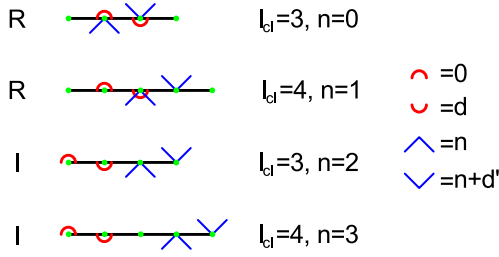
Figure 10: Linked clusters with size l_{cl} and with initial (half circles) and final (wedges) two-particle states for all addend in eqn. (13) at order $N = 4$ and for $d = d' = 1$. (I)R labels (ir)reducible graphs.

element from H_2, and depicts all $t_{d|n,d'}$ on their respective clusters including a label for reducing contributions to be evaluated according to eqns. (12, 13). These are $E_0^{cl}, t_{0,0}^{cl}, t_{1,1}^{cl}$ for $n = 0$ and $t_{0,2}^{cl}$ for $n = 1$ for this particular matrix element. Note that on finite clusters $t_{0,0}^{cl}$ and $t_{1,1}^{cl}$ are not necessarily identical. The one-particle irreducible matrix element from H_1 is straightforward. The complete matrix element reads

$$^0\langle q,1|H_1 + H_2|q,1\rangle^0 = 2 + \frac{1}{6}(j_1 + j_2) + \frac{431}{432}(j_1^2 + j_2^2)$$
$$- \frac{461}{216}j_1 j_2 + \frac{5827}{15552}(j_1^3 + j_2^3) - \frac{5725}{15552}(j_1^2 j_2 + j_1 j_2^2)$$
$$- \frac{18511597}{156764160}(j_1^4 + j_2^4) - \frac{51190589}{26127360}j_1^2 j_2^2$$
$$+ \frac{6030787}{5598720}(j_1^3 j_2 + j_1 j_2^3)$$

$$+ \left[-\frac{14}{27}(j_1^2 + j_2^2) + \frac{28}{27}j_1 j_2 - \frac{68}{243}(j_1^3 + j_2^3) \right.$$
$$+ \frac{68}{243}(j_1^2 j_2 + j_1 j_2^2) - \frac{23057}{17496}(j_1^3 j_2 + j_1 j_2^3)$$
$$\left. + \frac{72187}{349920}(j_1^4 + j_2^4) + \frac{21559}{9720}j_1^2 j_2^2 \right]\cos(q)$$
$$+ \left[\frac{76}{729}(j_1^4 + j_2^4) - \frac{493}{729}(j_1^3 j_2 + j_1 j_2^3) \right.$$
$$\left. + \frac{278}{243}j_1^2 j_2^2 \right]\cos(2q) \tag{18}$$

Finally, in the $Q = 2$ sector the single-particle states $|t_{1i}^m\rangle, |t_{2i}^m\rangle$, and $|s_{1i}\rangle$ need to be considered. Any one-particle irreducible Hamiltonian matrix element between the two- and one-particle states for $Q = 2$ is zero due to orthogonality. Two-particle irreducible contributions require matrix elements of the form

$$^{Sm}\langle q, d'|H_{eff}|q\rangle^{Sm} , \tag{19}$$

where $|q\rangle^{Sm} = \sum_r e^{iqr}|r\rangle^{Sm}/\sqrt{L}$ is a one-particle state of spin quantum numbers S, m with $Q = 2$. This implies a *decay* of $Q = 2$ single-particle states into $Q = 2$ two-particle states. *Up to the order that we have performed the SE, we have not observed such decay.* In turn the Hamiltonian matrix in the $Q = 2$ sector of the four-tube is already diagonal w.r.t. the particle number.

* Electronic address: w.brenig@tu-bs.de
[1] E. Dagotto and T. M. Rice, Science **271**, 618 (1996).
[2] M. Uehara, T. Nagata, J. Akimitsu, H. Takahashi, N. Mori, and K. Kinoshita, J. Phys. Soc. Jpn. **65**, 2764 (1996).
[3] E. Dagotto, Rep. Prog. Phys. **62**, 1525 (1999).
[4] D. C. Johnston, M. Troyer, S. Miyahara, D. Lidsky, K. Ueda, M. Azuma, Z. Hiroi, M. Takano, M. Isobe, Y. Ueda, et al., arXiv:cond-mat/0001147 (2000).
[5] F. D. M. Haldane, Phys. Rev. Lett. **50**, 1153 (1983).
[6] J. Schnack, H. Nojiri, P. Kögerler, G. J. T. Cooper, and L. Cronin, Phys. Rev. B **70**, 174420 (2004).
[7] H. Manaka, Y. Hirai, Y. Hachigo, M. Mitsunaga, M. Ito, and N. Terada, J. Phys. Soc. Jpn. **78**, 093701 (2009).
[8] V. O. Garlea, A. Zheludev, L.-P. Regnault, J.-H. Chung, Y. Qiu, M. Boehm, K. Habicht, and M. Meissner, Phys. Rev. Lett. **100**, 037206 (2008).
[9] A. Zheludev, V. O. Garlea, L.-P. Regnault, H. Manaka, A. Tsvelik, and J.-H. Chung, Phys. Rev. Lett. **100**, 157204 (2008).
[10] P. Millet, J. Y. Henry, F. Mila, and J. Galy, J. Solid State Chem. **147**, 676 (1999).
[11] K. Kawano and M. Takahashi, J. Phys. Soc. Jpn. **66**, 4001 (1997).
[12] T. Sakai, M. Sato, K. Okamoto, K. Okunishi, and C. Itoi, J. Phys.: Cond. Mat. **22**, 403201 (2010).
[13] J.-B. Fouet, A. Läuchli, S. Pilgram, R. M. Noack, and F. Mila, Phys. Rev. B **73**, 014409 (2006).
[14] S. Nishimoto and M. Arikawa, Phys. Rev. B **78**, 054421 (2008).
[15] D. Charrier, S. Capponi, M. Oshikawa and P. Pujol, Phys. Rev. B **82**, 075108 (2010).
[16] D. C. Cabra, A. Honecker, and P. Pujol, Phys. Rev. B **58**, 6241 (1998).
[17] E. H. Kim and J. Sólyom, Phys. Rev. B **60**, 15230 (1999).
[18] ALPS-Bibliothek, *http://alps.comp-phys.org*.
[19] C. Knetter and G. S. Uhrig, Eur. Phys. J. B **13**, 209 (2000).
[20] F. Wegner, Ann. Phys. **506**, 77 (1994).
[21] M. Arlego and W. Brenig, Eur. Phys. J. B **53**, 193 (2006).
[22] M. Arlego and W. Brenig, Phys. Rev. B **78**, 224415 (2008).
[23] M. Arlego and W. Brenig, Phys. Rev. B **75**, 024409 (2007).
[24] W. Brenig and M. Grzeschik, Phys. Rev. B **69**, 064420 (2004).
[25] W. Brenig and A. Honecker, Phys. Rev. B **65**, 140407(R) (2002).
[26] W. Brenig, Phys. Rev. B **67**, 064402 (2003).
[27] This expressions are too long to be printed explicitely. Upon request they will be made available electronically.
[28] C. Jurecka and W. Brenig, Phys. Rev. B **61**, 14307 (2000).
[29] S. Trebst, H. Monien, C. J. Hamer, Z. Weihong, and R. R. P. Singh, Phys. Rev. Lett. **85**, 4373 (2000).

[30] C. Knetter, K. P. Schmidt, M. Grüninger, and G. S. Uhrig, Phys. Rev. Lett. **87**, 167204 (2001).

[31] W. Zheng, C. J. Hamer, R. R. P. Singh, S. Trebst, and H. Monien, Phys. Rev. B **63**, 144410 (2001).

[32] W. Brenig and K. W. Becker, Phys. Rev. B **64**, 214413 (2001).

[33] C. Knetter, K. P. Schmidt, and G. S. Uhrig, Eur. Phys. J. B **36**, 525 (2004).

[34] K. P. Schmidt, C. Knetter, and G. S. Uhrig, Phys. Rev. B **69**, 104417 (2004).